Food Chemistry: X 19 (2023) 100829

Contents lists available at ScienceDirect

Food Chemistry: X

journal homepage: www.sciencedirect.com/journal/food-chemistry-x

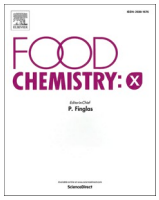

Improving the quality of soluble dietary fiber from *Poria cocos* peel residue following steam explosion

Tianlin Wang [a], Zhongshan Xiao [b], Tiange Li [a], Ge Guo [a], Suyun Chen [c], Xianqing Huang [a,*]

[a] Henan Engineering Technology Research Center of Food Processing and Circulation Safety Control, College of Food Science and Technology, Henan Agricultural University, Zhengzhou 450002, Henan, China
[b] Department of Pharmacy, Puyang Medical College, Puyang 457000, Henan, China
[c] College of Economics and Management, Henan Agricultural University, Zhengzhou 450002, Henan, China

ARTICLE INFO

Keywords:
Poria cocos peel residue
Steam explosion
Soluble dietary fiber

ABSTRACT

Poria cocos peel residue (PCPR) still contains much soluble dietary fiber (SDF), steam explosion (SE) treatment was applied to PCPR to create a superior SDF. Steam pressure of 1.2 MPa, residence period of 120 s, and moisture content of 13% were the optimized parameters for SE treatment of PCPR. Under optimized circumstances, SE treatment of PCPR enhanced its SDF yield from 5.24% to 23.86%. Compared to the original SDF, the SE-treated SDF displayed improved enzyme inhibition, including the inhibition of α-amylase and pancreatic lipase, also enhanced water holding, oil holding, water swelling, nutrient adsorption including cholesterol, nitrite ions, and glucose and antioxidant abilities. Additionally, it had a decreased molecular weight, improved thermal stability, and a rough surface with many pores of different sizes. Given that SDF had been improved physiochemical and functional characteristics thanks to SE treatment, it might be the excellent functional ingredient for the food business.

1. Introduction

Poria cocos is an eatable fungus that is primarily grown in China. Due to the mushroom's high concentration of polysaccharides, triterpenoids, dietary fibers (DFs), proteins, trace elements, and amino acids, it has therapeutic benefits on inflammation, oxidative stress, tumors, and hyperglycemia (Zhao et al., 2023). So, after processing, *Poria cocos* is typically consumed as food or used as medicine (Lan et al., 2023). The *Poria cocos* peel residue (PCPR), produced as a by-product of processing of *Poria cocos* is typically discarded or utilized as animal feed. However, PCPR is abundant in DF, as a result, it might have additional economic worth. DF, as a kind of macromolecular polysaccharide, is one of the seven nutrients. In the small intestine, it is not, however, absorbed (Nepali et al., 2022). According to studies, DF lowers the risk of developing some prolonged ailments, such as heart disease (Khanpit et al., 2022), diabetes (Mazhar et al., 2023) and obesity (Waddell & Orfila, 2022). Based on its solubility, DF can be divided into two categories: insoluble DF and soluble DF (SDF) (Liu et al., 2022; Gan et al., 2020). The surface shape, functional groups, and molecular weight of SDF are typically significant contributors in the physical, chemical and functional characteristics of DF. High-quality DF has an SDF concentration of more than 10% (Khanpit et al., 2021; Qiao et al., 2021). For the sake of reusing PCPR, boosting the SDF content in DF might be one option.

The process known as steam explosion (SE) is a common physical pretreatment in which fibrous raw materials are treated with high temperature pressurized steam for a set amount of time. This pushes the steam into the raw materials' tissues and cells to achieve component separation and mechanical alteration in the materials through the prompt pressure relief procedure (Nader et al., 2022; Wan et al., 2022). SE is better than other pretreatment techniques in terms of affordability, energy efficiency, and absence of chemical pollution (Arshanitsa et al., 2022). During SE processing, cellulose and hemicellulose, which are insoluble macromolecular polysaccharides, are converted into the small-molecule soluble polysaccharide SDF either through thermal degradation or hydrogen bond breaking (Arshanitsa et al., 2022). Therefore, SDF extract yield from by-products including orange peel (Fan et al., 2022), sweet potato waste (Wang et al., 2017), okara (Li et al., 2019) and apple pomace (Zhao et al., 2022), has been improved using SE technology. These results suggest that SE could be used as a pretreatment method to produce high quality SDF from PCPR.

To achieve the highest SDF extraction yield in the current work, PCPR was treated with SE utilizing certain experimental conditions. To

* Corresponding author.
E-mail address: hxq8210@126.com (X. Huang).

https://doi.org/10.1016/j.fochx.2023.100829
Received 25 November 2022; Received in revised form 31 July 2023; Accepted 5 August 2023
Available online 7 August 2023

ascertain if this unique approach may aid in making full use of PCPR, the physicochemical parameters, functional properties, and microstructures of original SDF and SE-treated SDF (hereinafter referred to as O-SDF and SE-SDF) were further assessed.

2. Materials and methods

2.1. Raw materials and reagents

Chenguang Biotechnology Co., Ltd. Handan, China was considered for the purchase the *Poria cocos* peel residue. Shanghai Yuanye Biotechnology Co., Ltd. supplied pancreatic lipase (30 U/mg), α-amylase (30 U/mg), and alkaline protease (100 U/mg) (Shanghai, China). Kermel Chemical Reagent Co. Ltd. (Tianjin, China) was used for the purchase of analytical grade of all other chemicals and reagents.

2.2. SE processing

A 500 mL cylinder-piston arrangement was used to load 300 g of dried PCPR into the reactor chamber of the SE machine (QBS-80, Zhengdao Bioenergy Co. Ltd., Hebi, China). The reactor chamber was then filled with vapor that had moisture contents of 7, 9, 11, 13 and 15% and high-pressure steam (0.3, 0.6, 0.9, 1.2, 1.5, and 1.8 MPa) that was sustained for a predetermined amount of time (60, 120, 180, 240 and 300 s). The steam inlet was then closed, and within 0.0875 s the piston device was activated for the explosive depressurization (Wang et al., 2017). The collected SE-treated PCPR were dried at 65 °C in a drying oven (GZX-9023MBE, Thermo, USA), and stored at room temperature in a desiccator.

2.3. Preparation of SDF from PCPR

The AOAC 991.43 approach served as the foundation for the creation of SDF. The original PCPR and SE-treated PCPR was submerged in n-hexane (1:5, w/v) for 2 h. For the purpose of removing starch and protein, the sample was first successively hydrolyzed by α-amylase (pH 6.5, 55 °C water bath for 1 h), amyloglucosidase (pH 4.5, 55 °C water bath for 1 h), and alkaline protease (pH 9.0, 55 °C water bath for 1 h). Then, the mixture was heated at 95 °C for 10 min to deactivate the enzymes. After 12 h at 4 °C, the mixture was centrifuged at 8000*g* for 10 min to obtain supernatant. Next, the supernatant was mixed in a 1:4 ratio with 95 percent (v/v) ethanol and centrifuged at 8000*g* for 10 min. The precipitates were dried at 65 °C. Finally, the sample was milled and sieved through a 60-mesh sieve to obtain SDF with uniform particle size.

2.4. Physicochemical properties

2.4.1. Water holding capacity (WHC)

With some slight modifications, the Liu et al. (2021) approach served as the foundation for the measurement of WHC. 20 mL of distilled water were mixed with 0.5 g SDF for a day at ambient temperature. After that, the mixture was centrifuged at 8000*g* for 6 min. The collected wet SDF was weighed and recorded as mass M_1. Then, the SDF was weighed and recorded as M_2 again after it had dried to a steady weight. The final equation for calculating WHC was as follows:

$$\mathrm{WHC}\ (\mathrm{g/g}) = (\mathrm{M_1} - \mathrm{M_2})/\mathrm{M_2}$$

2.4.2. Oil holding capacity (OHC)

With a few modest modifications, the Huang et al. (2021) approach served as the foundation for the OHC measurement. 10 mL of soybean oil was mixed with SDF (0.5 g) for 18 h at room temperature, followed by a 6 min centrifugation at 8000×g. The weight of the collected residue was then recorded as M1, and M2 represented the bulk of the dried residue. The final equation for calculating OHC was as follows:

$$\mathrm{OHC(g/g)} = (\mathrm{M_1} - \mathrm{M_2})/\mathrm{M_2}$$

2.4.3. Water swelling capacity (WSC)

With a few minor modifications, the WSC was measured utilizing technique of Chen et al (2021). A graduated cylinder was filled with SDF (0.5 g, M_0), and the initial volume of the sample was noted as V_1. The graduated cylinder was then filled with 10 mL of distilled water and left at room temperature for 18 h. Following this, V_2 was recorded as the final volume of the hydrated sample in the graduated cylinder. WSC was determined using the following equation:

$$\mathrm{WSC}\ (\mathrm{mL/g}) = (\mathrm{V_1} - \mathrm{V_2})/\mathrm{M_0}$$

2.5. Functional properties

2.5.1. Cholesterol adsorption capacity (CAC)

The CAC was calculated using technique developed by Ma et al (2021) with minimal modifications. 5 mL of yolk of an egg was mixed with 45 mL of distilled water to create an emulsion. 0.5 g of SDF and 10 mL of emulsion were combined and shaken using a vortex mixer (Vortex-3000, WIGGENS, Germany) at room temperature for 6 h. The supernatant was collected after centrifugation at 1000*g* for 10 min. Glacial acetic acid was combined with the obtained supernatant (1:10, v/v) to from uniform solution. Then, the weight of the solution was used to determine the cholesterol content. The egg yolk emulsion without the SDF sample was used as the blank. The following equation was used to compute the CAC:

$$\mathrm{CAC}\ (\mathrm{mg/g}) = (\mathrm{M_1} - \mathrm{M_2})/\mathrm{M_0}$$

M_0 represented the weight of the SDF sample, while M_1 and M_2 represented the weight of the emulsion before and after it had been applied to the SDF.

2.5.2. Nitrite ion adsorption capacity (NIAC)

The Zheng et al. (2021) technique was used to calculate the NIAC with a few minor modifications. A 10 mL solution of $NaNO_2$ (0.1 mg/mL) with pH values of 2.0 and 7.0 was initially mixed with 0.5 g of SDF to mimic the environment of the small intestine and stomach. After being left at room temperature for 2 h, the mixture was centrifuged for 10 min at 8000*g*. Next, 1 mL of the supernatant was added into 4 mL of *p*-aminobenzene sulfonic acid (10 μg/mL) and 4 mL of HCl naphthodiamide (5 μg/mL), then the mixture was incubated for 1 h under ambient temperature. An ultraviolet spectrophotometer (AQ8100, Thermo, USA) was used to determine the absorption spectra of $NaNO_2$ at wavelength of 538 nm, and then the weight of $NaNO_2$ was estimated using the standard curve. The NIAC was calculated using the following equation.

$$NIAC(\mu g/g) = (M_1 - M_2)/M_0$$

M_0 was the weight of the SDF sample, and M_1 and M_2 represented the weights of $NaNO_2$ in the solution prior to and following adsorption.

2.5.3. Glucose absorption capacity (GAC)

With a few minor modifications, the GAC was measured using Hu et al. (2022) methodology. 20 mL of glucose solution (20 mM) and 0.5 g of SDF were combined, and 8 h were spent stirring in a thermostat water bath at 37 °C. The mixture was then spun at 8000*g* for 10 min. A commercially available glucose test kit was used to measure the amount of glucose in the supernatant (Abcam, Shanghai, China). The following equation was used to determine the GAC:

$$GAC(\mu mol/g) = (C_1V_1 - C_2V_2)/M$$

where C_1 is the added glucose concentration, V_1 is the added glucose volume, C_2 is the added glucose concentration in the supernatant, V_2 is the added glucose supernatant volume, and M is the weight of the SDF

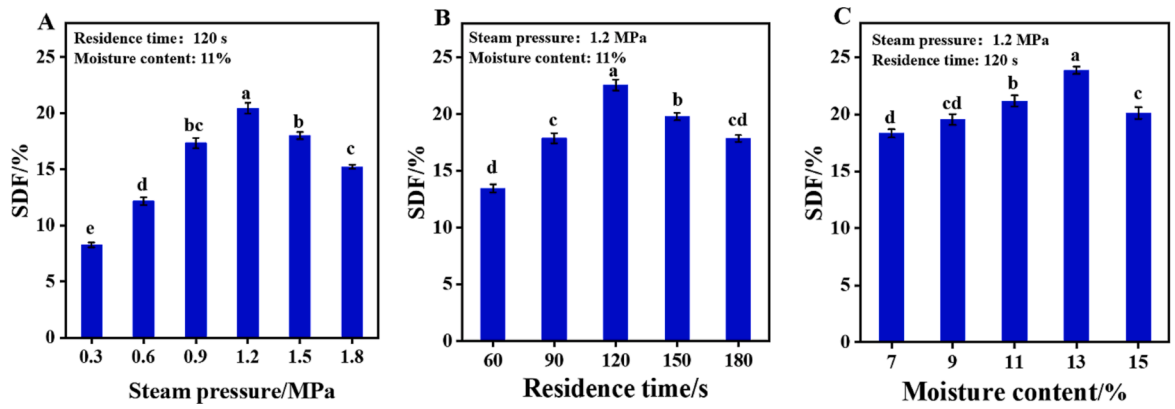

Fig. 1. SE parameter effects on SDF yield. (A) PCPR treated by SE at different steam pressures for 120 s and 11% moisture, (B) PCPR treated by SE at 1.2 MPa and 11% moisture at different residence times, (C) PCPR treated by SE at 1.2 MPa and 120 s at different moisture contents. Different letters indicate significant differences ($p < 0.05$).

sample.

2.5.4. Scavenging ability of hydroxyl radical (•OH) (SA-HR)

The Wang et al. (2022) approach served as the foundation for the SA-HR with some minor modifications. SDF (0.1–0.5 g) was dissolved in a 2.5 mL, 10 mM mixture of salicylic acid and ethanol, along with ferrous sulphate (2.5 mL, 10 mM). The combined solution was then given 0.1 mL of 10 mM hydrogen peroxide, and incubated for 45 min at 37 °C. An ultraviolet spectrophotometer was used to measure the solution's absorbance at 510 nm. Hydrogen peroxide was substituted with pure water as the control. The following equation was used to calculate the SA-HR:

$$\text{SA}-\text{HR}\ (\%) = [1-(\text{A}_1-\ \text{A}_2)/\text{A}_0] \times 100\%$$

where A_0 represented the absorbance of the control, A_1 represented the absorbance of the hydrogen peroxide-containing combination, and A_2 represented the absorbance of the hydrogen peroxide-free mixture.

2.5.5. Scavenging activity of 2,2-diphenyl-1-picrylhydrazyl (DPPH) radical (SA-DPPHR)

With some slight modifications, the SA-DPPHR was calculated using Ma et al. (2023) methodology. SDF (0.1–0.5 g) was dissolved in DPPH alcohol solution (10 mL, 1.0 mM) and stirred continuously for 2 h while it remained dark. Using a UV spectrophotometer, the mixture's absorbance was determined at 510 nm. Instead of the DPPH alcohol solution, distilled water was used as the control. The following equation was used to determine the SA-DPPHR:

$$\text{SA}-\text{DPPHR}\ (\%) = [1-(\text{A}_1-\ \text{A}_2)/\text{A}_0] \times 100\%$$

where A_0 was the DPPH solution absorbance, A_1 was the SDF dispersed in DPPH solution absorbance, and A_2 was the SDF dissolved in distilled water absorbance.

2.5.6. Inhibition ability of α-amylase (α-AAIR)

The method of Zheng et al. (2022) was slightly modified to measure the α-AAIR. 50 mL of soluble corn starch solution (4%, w/v) was added after adding SDF (0.5 g) and 1 mL of α-amylase solution (30 U/mL) to it. After being agitated for 2 h at 37 °C in a water bath, the mixture was centrifuged for 10 min at 8000*g*. A commercial glucose assay kit was used to determine the amount of glucose present in the supernatant. The samples without SDF added as control group. The percentage difference between the SDF added and control group's rate of glucose production was used to determine the α-AAIR.

2.5.7. Inhibition ability of pancreatic lipase (PLAIR)

The PLAIR was calculated using a slightly modified version of the Yang et al. (2022) approach. 0.5 g of SDF was combined with 5 mL of olive oil and shaken for 2 min, and then was added to 25 mL of sodium phosphate buffer (10 mM, pH 7.0) containing pancreatic lipase (10 U/mL). After being agitated in a water bath at 40 °C for 2 h, the mixture was heated to 95 °C for 10 min to inactivate. The samples without SDF added as control group. The percentage reduction in free acid generation rate relative to the control was used to determine the PLAIR.

2.6. Structural characteristics

2.6.1. Scanning electron microscopy (SEM)

A scanning electron microscope was used to look at the morphology of the SDF samples (SU9000, Hitachi, Japan). For SEM visualization, the SDF samples were mounted on double-sided tape and covered with a thin layer of gold. The photos were taken at 1.5x magnification and an accelerating voltage of 10 kV.

2.6.2. Fourier-transform infrared spectroscopy (FT-IR)

A FT-IR spectrometer was used to measure the spectra of SDF samples (Nicolet 6700, Thermo Fisher). 100 mg of KBr and 1 mg of SDF were combined. With a resolution of 4 cm^{-1} and 32 scans, FT-IR spectra in the wavenumber range of 400–4000 cm^{-1} were recorded.

2.6.3. X-ray diffraction (XRD)

By using XRD, the crystalline configuration of SDF samples was evaluated. A D8 X-ray diffractometer (Bruker AXS, Karlsruhe, Germany) was used to characterize the XRD spectrum while emitting Cu K α radiation at a 40 kV operating voltage and a 40 mA applied current. The diffraction angle (2θ), which was set to vary from 10° to 80°, was scanned at a rate of 1°/min.

2.6.4. Thermal properties

A thermos-gravimetric analyzer was used to assess the SDF samples' differential scanning calorimetry (DSC) (DSC 3500 Sirius, Netzsch, Selb, Germany). At a rate of 20 °C/min, samples were conducted at temperatures ranging from 30 to 300 °C. With a flow rate of 20 mL/min, high-purity nitrogen was employed to purge the system.

2.6.5. Specific surface area

A laser particle size analyzer was used to assess the SDF samples' specific surface area (Mastersizer-2000, Malvern, U.K.).

2.6.6. Molecular weight (Mw)

High-performance gel permeation chromatography was used to determine the molecular weight of SDF samples (HPGPC). In the mobile phase, the SDF and dextran standards were dispersed and shaken for 5

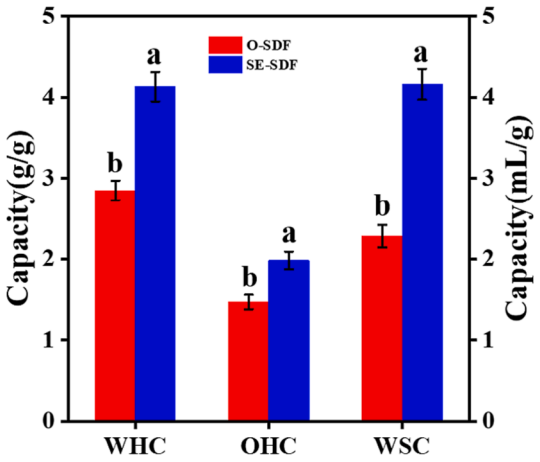

Fig. 2. SE parameters effect on WSC, OHC and WHC in SE-SDF and O-SDF. Different letters indicate significant differences ($p < 0.05$).

min. After that, a 0.22 μm membrane filter was used to filter the solution. In accordance with the standard curve created by the T-series Dextran standard, the molecular weight of the SDF samples was determined.

2.7. Statistical analyses

All experiments were performed at least in triplicate and the results were presented as mean ± standard deviation. One-way analysis of variance (ANOVA) was performed using IBM SPSS statistical software (version 21.0, SPSS Inc., Chicago, IL, USA). Significant differences ($p < 0.05$) of means were determined by the Tukey test.

3. Results and discussion

3.1. SE parameters effect on yield of SDF

The SDF yield achieved from PCPR was impacted by the steam pressure used during preprocessing with the residence time (120 s) and moisture content (11%): from 0.3 and 1.2 MPa, the SDF yield increased from 8.27% to 20.46%, whereas above 1.2 MPa, the SDF yield dropped (Fig. 1A). The yield of SDF was known to be decreased by the degradation and conversion of cellulose, hemicellulose, and lignin into tiny molecules (Fan et al., 2022). When the residence period was up to 120 s under 1.2 MPa pressure with the moisture content of 11%, the SDF yield reached its maximum level (22.56%) (Fig. 1B). However, while the high pressure treatment continues, the macromolecule polysaccharide was continually broken down into small molecules, lowering the generation of SDF (Zhang et al., 2022). Fig. 1C illustrated the impact of moisture content on SDF yield after SE. At 1.2 MPa pressure and 120 s residence time, respectively, the SDF yield rose and peaked at 23.86% with a moisture content of 13%. Notably, excessive moisture resulted in the PCPR sticking together, which prevented water vapor from fully penetrating the material, leaving the SE process unfinished and reducing the SDF yield. Under the ideal circumstances outlined above, the yield of SE-SDF (23.86%) was much higher than that of O-SDF (5.24%). And the results also showed that the content of SDF in PCPR after SE treatment was significantly higher than that after twin-screw extrusion (TSE) treatment and ultrafine grinding (UG) treatment (Fig. S1).

3.2. Physicochemical properties of SDF

SE parameters effect on WSC, OHC and WHC in SDF were shown in Fig. 2. When compared to O-SDF, the WHC and OHC in SE-SDF increased from 2.85 to 4.13 g/g and from 1.47 to 1.98 g/g, respectively, as a result

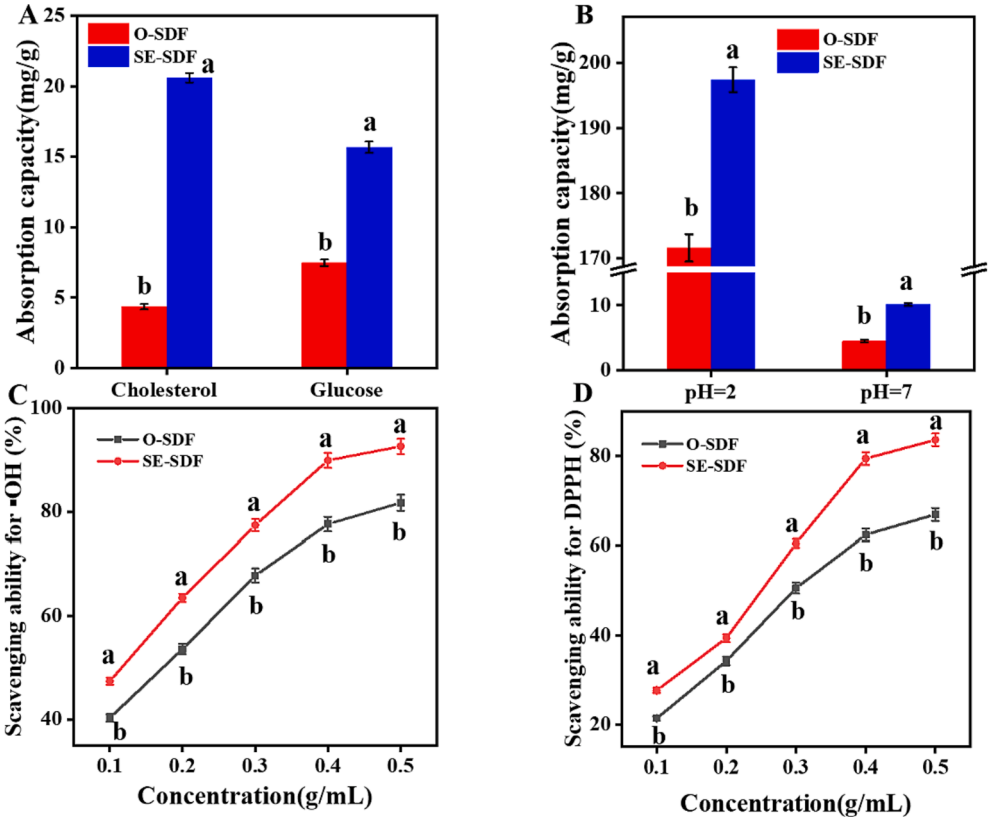

Fig. 3. SE parameters effect on CAC and GAC (A), NIAC (B), SA-HR (C), SA-DPPHR (D) in SE-SDF and O-SDF. Different letters indicate significant differences ($p < 0.05$).

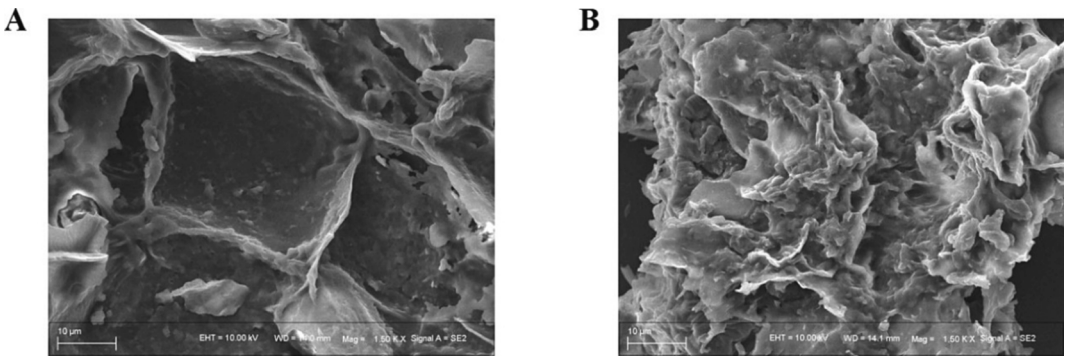

Fig. 4. The SEM of O-SDF (A) and SE-SDF (B) from PCPR.

of the modified three-dimensional structure of SDF and the addition of short-chain DF. Likely due to SE's induction of the DF's porous and rough surface (Wang et al., 2017), the WSC in SE-SDF rose from 2.28 to 4.16 mL/g. Similar results were observed in earlier studies that focused on SDF that had undergone twin-screw extrusion (Qiao et al., 2021) and superfine grinding processing (Zhu et al., 2022).

3.3. Functional properties of SDF

3.3.1. CAC, GAC and NIAC

The CAC of SDF was a significant marker of the fiber's capacity to lower serum cholesterol levels and prevent human cardiovascular disease. Another crucial characteristic of SDF was its ability to combine with glucose in intestinal juice to lower the levels of postprandial blood glucose (Si et al., 2022). The CAC and GAC of SE-SDF dramatically increased from 4.35 to 20.59 mg/g and from 7.47 to 15.69 mg/g, respectively, in comparison to the CAC and GAC of O-SDF (Fig. 3A). Under the influence of gastric acid, nitrite can combine with the secondary amines of protein breakdown products to generate nitrosamine. Nitrosamines have a potent carcinogenic effect and are linked to an increased risk of esophageal, gastric, liver, and colorectal cancers (Zheng et al., 2021). As a result, the NIAC of SDF was determined, Fig. 3B displayed the NIAC values of SDF samples in simulated gastric settings with a pH of 2.0 and small intestinal environment with a pH of 7.0. The NIAC values of SE-SDF at pH levels of 2.0 and 7.0 were much higher than those of O-SDF, at 197.4 and 10.1 g/g, respectively. The greater specific surface area of SE-SDF and its more intricate structure, which enhanced the binding of cholesterol and glucose, were responsible for these outcomes.

3.3.2. SA-DPPHR and SA-HR

The frequency of •OH interactions with biological macromolecules increased when the body has an excess of it, which could lead to disorders associated with oxidative stress (Qiao et al., 2021). SDF was a top choice for scavenging free radicals. Fig. 3C demonstrated that as the amount of SDF rose from 0.1 to 0.5 g, SE-SDF had stronger SA-HR than O-SDF (21.4% -66.9%) did. It was considered that DPPH was the one of gold standard for assessing the capacity of natural compounds to scavenge free radicals (Qiao et al., 2021). According to Fig. 3D, the SA-DPPHR of SE-SDF (47.4% to 95.6%) outperformed O-SDF (40.3% to 81.7%) when SDF concentration increased. The results were probably caused by SE-lower SDF's molecular weight, which increased the antioxidant activity of SDF (Li et al., 2022).

3.3.3. α-AAIR and PLAIR

Studies have shown that SDF inhibits enzyme degradation to reduce the release rate of substances in food, and the viscous food mass formed by SDF can hinder the digestion and absorption of starch, fat, and other substances, which helps control the rise of postprandial blood sugar (Turner & Lupton, 2021). As shown in Fig. S2, SE-SDF exerted higher α-AAIR (12.34%) and PLAIR (15.68%) than O-SDF (α-AAIR: 5.95%; PLAIR: 8.74%). The changes in the microstructure and increases in surface area of SE-SDF likely captured more enzymes and substrates, reducing the accessibility between the enzymes and substrates (Zheng et al., 2022).

3.4. Structural properties of SDF

3.4.1. Microtopography analysis

SEM was used to view the microstructure of SDF from PCPR (Fig. 4). O-SDF had a surface that was mostly plane and even (Fig. 4A), but SE-SDF had a rough external with several holes of different sizes that increased its surface area (Fig. 4B). This structural shift resulted from the SE treatment's breakdown of the glycosidic linkages in various macromolecular polysaccharides, including cellulose and lignin. In a prior work, SE treatment improved the binding and adsorption capacity of SDF (Shen et al., 2019).

3.4.2. FTIR analysis

FTIR was used to examine the spectroscopic characteristics and chemical makeup of the functional groups of SDF from PCPR. As seen in Fig. S3, aside from minor differences in absorption strength, the majority of the distinctive peaks of O-SDF and SE-SDF were comparable. In contrast to the weaker peak in SE-SDF at 3442 cm^{-1}, which suggested that hemicellulose and cellulose were broken with an increase in hydrophilicity. The two wide peaks in both SDFs were measured at 3392–3442 cm^{-1} and assigned to –OH stretching in cellulose and hemicellulose (Huang et al., 2018). The stretching vibration of the C-H atom in the methyl and methylene groups was said to be the cause of the peaks about 2935 cm^{-1}. A distinct peak at 1430 cm^{-1} was observed in SE-SDF as opposed to the peak at 1429 cm^{-1} in O-SDF, which was most likely caused by the increased amount of uronic acid (Chylinska et al., 2016). It was determined that the stretching vibrations of the C-O-H and C-O-C structures in glucopyranose were responsible for the peaks at 960 and 1145 cm^{-1} (Chen et al., 2018).

3.4.3. Crystalline structure

Fig. S4 depicted the crystalline structure of SDF following SE treatment. O-SDF and SE-conspicuous SDF's diffraction peaks were observed at 21.1°, matching the natural cellulose type I crystal structure, which coexisted with amorphous and crystalline regions (Zhai et al., 2022). According to the XRD patterns, the crystal-type SDF samples had not been changed by SE treatment. Furtherly, the relative CrI of SE-SDF and O-SDF were calculated by the Segal formula. However, the CrI of SE-SDF decrease to 25.47%, compared with that of O-SDF (29.66%). It might be owing to the explosion during SE destroyed partial crystalline region of SDF, transforming the crystalline region into the amorphous region (Zhai et al., 2022).

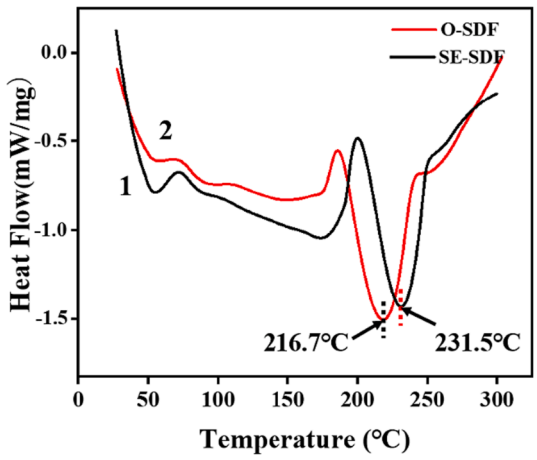

Fig. 5. The thermal analysis of O-SDF (2) and SE-SDF (1) from PCPR.

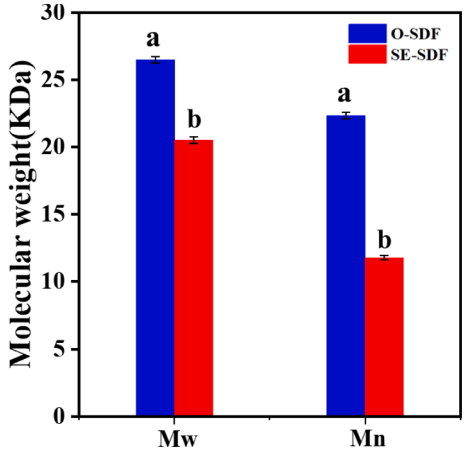

Fig. 6. The molecular weight distributions of O-SDF and SE-SDF from PCPR. Different letters indicate significant differences ($p < 0.05$). Mw: Weight-average molecular weight; Mn: Number-average molecular weight.

3.4.4. Thermal characteristics

Fig. 5 showed the DSC spectrum of the SDF samples. Two usual endothermic peaks for O-SDF and SE-SDF were located at 216.7° and 231.5°, respectively. After SE treatment, SE-SDF had strong hydrogen bonds within its junction zones that require more energy to decompose its crystalline structure, leading to the increase in the thermal stability of SE-SDF (Qiao et al., 2021).

3.4.5. Specific surface area determination

A prior investigation revealed that SDF's specific surface area was crucial to both its physicochemical and functional characteristics (Zhang et al., 2023). After SE treatment, the particular surface region of SDF rose 2.93 times, from 73.3 m^2/kg (that of O-SDF) to 214.6 m^2/kg (that of SE-SDF). These findings, which were in line with the findings of the SEM study, may help to explain the enhanced physicochemical and functional characteristics of SE-SDF.

3.4.6. Molecular weight (Mw) determination

The HPGPC technique was applied to calculate molecular weight of the SDF samples. Both O-SDF and SE-SDF showed several peaks and different molecular weights as the retention period was prolonged in accordance to the observed chromatograms. O-SDF and SE-SDF had initial molecular weights of 26.47 and 20.52 KDa, respectively, as presented in Fig. 6. SE treatment resulted in a 22.3% reduction in the molecular weight of SE-SDF. This finding confirmed the breakdown of cellulose and hemicellulose molecular chains brought on by SE treatment's elevated pressure and temperature, which lowered the molecular polymerization and raised solubility (Spann & Boucher, 2022).

4. Conclusions

To increase the yield of its SDF, the PCPR was treated with SE in the current investigation under ideal circumstances (steam pressure, 1.2 MPa; residence time, 120 s; moisture content, 13 percent). The yield of SDF dramatically enhanced under these optimized conditions. The SE-SDP that was produced had excellent physicochemical and functional characteristics. For instance, SE-SDF significantly outperformed O-SDF in terms of WHC, OHC, WSC, CAC, NIAC, GAC, -AAIR, PLAIR, SA-HR, and SA-DPPHR values. Using SEM, FTIR, XRD, HPGPC, and TA analyses, the structural characteristics of SE-SDF and O-SDF were also characterized. The results showed that, despite having similar crystalline structures and characteristic peaks, SE-SDF had a coarser surface and a lower molecular weight with higher thermal stability than O-SDF. The SDF derived from SE-treated PCPR had optimal physiological activity and acceptable adsorption, indicating that it might be employed as a functional additive in the food sector. As a result, the current findings suggested that SE treatment will enabled the reuse of PCPR.

CRediT authorship contribution statement

Tianlin Wang: Methodology, Resources, Conceptualization, Writing – original draft. **Zhongshan Xiao:** Methodology, Software. **Tiange Li:** Conceptualization, Funding acquisition. **Ge Guo:** Formal analysis. **Suyun Chen:** Resources. **Xianqing Huang:** Supervision, Writing – review & editing.

Declaration of Competing Interest

The authors declare that they have no known competing financial interests or personal relationships that could have appeared to influence the work reported in this paper.

Data availability

Data will be made available on request.

Acknowledgements

This work was supported by the Natural Science Foundation of Henan Province (NO. 232300421259), the National Natural Science Foundation of China (NO. 32101966), 2022 Henan postgraduate joint training base project (NO. YJS2022JD16) and the Program for Innovative Research Team (in Science and Technology) in university of Henan Province (NO. 23IRTSTHN023).

Appendix A. Supplementary data

Supplementary data to this article can be found online at https://doi.org/10.1016/j.fochx.2023.100829.

References

Arshanitsa, A., Ponomarenko, J., Lauberte, L., Jurkjane, V., Pals, M., Akishin, Y., … Telysheva, G. (2022). Advantages of MW-assisted water extraction, combined with steam explosion, of black alder bark in terms of isolating valuable compounds and energy efficiency. *Industrial Crops and Products, 181*. https://doi.org/10.1016/j.indcrop.2022.114832

Chen, H., Xiong, M., Bai, T., Chen, D., Zhang, Q., Lin, D., … Qin, W. (2021). Comparative study on the structure, physicochemical, and functional properties of dietary fiber extracts from quinoa and wheat. *LWT, 149*. https://doi.org/10.1016/j.lwt.2021.111816

Chen, H., Zhao, C., Li, J., Hussain, S., Yan, S., & Wang, Q. (2018). Effects of extrusion on structural and physicochemical properties of soluble dietary fiber from nodes of lotus root. *LWT, 93*, 204–211. https://doi.org/10.1016/j.lwt.2018.03.004

Chylinska, M., Szymanska-Chargot, M., & Zdunek, A. (2016). FT-IR and FT-Raman characterization of non-cellulosic polysaccharides fractions isolated from plant cell wall. *Carbohydrate Polymers, 154*, 48–54. https://doi.org/10.1016/j.carbpol.2016.07.121

Fan, R., Wang, L., Fan, J., Sun, W., & Dong, H. (2022). The pulsed electric field assisted-extraction enhanced the yield and the physicochemical properties of soluble dietary fiber from orange peel. *Frontiers in Nutrition, 9*, Article 925642. https://doi.org/10.3389/fnut.2022.925642

Gan, J., Peng, G., Liu, S., Hu, X., Wang, X., Guo, S., … Yu, Q. (2020). Comparison of structural, functional and in vitro digestion properties of bread incorporated with grapefruit peel soluble dietary fibers prepared by three microwave-assisted modifications. *Food & Function, 11*(7), 6458–6466. https://doi.org/10.1039/d0fo00760a

Hu, K., Chen, D., & Sun, Z. (2022). Structures, physicochemical properties, and hypoglycemic activities of soluble dietary fibers from white and black glutinous rice bran: A comparative study. *Food Research International, 159*, Article 111423. https://doi.org/10.1016/j.foodres.2022.111423

Huang, J. Y., Liao, J. S., Qi, J. R., Jiang, W. X., & Yang, X. Q. (2021). Structural and physicochemical properties of pectin-rich dietary fiber prepared from citrus peel. *Food Hydrocolloids, 110*, Article 106140. https://doi.org/10.1016/j.foodhyd.2020.106140

Huang, L., Ding, X., Zhao, Y., Li, Y., & Ma, H. (2018). Modification of insoluble dietary fiber from garlic straw with ultrasonic treatment. *Journal of Food Processing and Preservation, 42*(1), 13399. https://doi.org/10.1111/jfpp.13399

Khanpit, V. V., Tajane, S. P., & Mandavgane, S. A. (2021). Dietary fibers from fruit and vegetable waste: Methods of extraction and processes of value addition. *Biomass Conversion and Biorefinery, 1–20*. https://doi.org/10.1007/s13399-021-01980-2

Khanpit, V. V., Tajane, S. P., & Mandavgane, S. A. (2022). Extrusion for soluble dietary fiber concentrate: Critical overview on effect of process parameters on physicochemical, nutritional, and biological properties. *Food Reviews International, 1–22*. https://doi.org/10.1080/87559129.2022.2097689

Lan, K., Yang, H., Zheng, J., Hu, H., Zhu, T., Zou, X., … Liu, H. (2023). Poria cocos oligosaccharides ameliorate dextran sodium sulfate-induced colitis mice by regulating gut microbiota dysbiosis. *Food & Function, 14*, 857–873. https://doi.org/10.1039/D2FO03424G

Li, B., Yang, W., Nie, Y., Kang, F., Goff, H. D., & Cui, S. W. (2019). Effect of steam explosion on dietary fiber, polysaccharide, protein and physicochemical properties of okara. *Food Hydrocolloids, 94*, 48–56. https://doi.org/10.1016/j.foodhyd.2019.02.042

Li, J., Yang, Z., Zhang, Y., Gao, B., Niu, Y., Lucy, Y.u., & L.. (2022). The structural and functional characteristics of soluble dietary fibers modified from tomato pomace with increased content of lycopene. *Food Chemistry, 382*, Article 132333. https://doi.org/10.1016/j.foodchem.2022.132333

Liu, J., Hua, J., Chen, S., Zhao, L., Wang, Q., & Zhou, A. (2022). The potential mechanisms of bergamot-derived dietary fiber alleviating high-fat diet-induced hyperlipidemia and obesity in rats. *Food & Function, 13*(15), 8228–8242. https://doi.org/10.1039/d2fo00747a

Liu, Y., Zhang, H., Yi, C., Quan, K., & Lin, B. (2021). Chemical composition, structure, physicochemical and functional properties of rice bran dietary fiber modified by cellulase treatment. *Food Chemistry, 342*, Article 128352. https://doi.org/10.1016/j.foodchem.2020.128352

Mazhar, M., Zhu, Y., & Qin, L. (2023). The interplay of dietary fibers and intestinal microbiota affects type 2 diabetes by generating short-chain fatty acids. *Foods, 12*(5), 1023. https://10.3390/foods12051023.

Ma, R., Chen, J., Zhou, X., Lin, H., Gao, Q., Peng, X., … Xue, Y. (2021). Effect of chemical and enzymatic modifications on the structural and physicochemical properties of dietary fiber from purple turnip (Brassica rapa L.). *LWT, 145*. https://doi.org/10.1016/j.lwt.2021.111313

Ma, Z., Zhai, X., Zhang, N., & Tan, B. (2023). Effects of germination, fermentation and extrusion on the nutritional, cooking and sensory properties of brown rice products: A comparative study. *Foods, 12*(7), 1542. https://10.3390/foods12071542.

Nader, S., Brosse, N., Daas, T., & Mauret, E. (2022). Lignin containing micro and nano-fibrillated cellulose obtained by steam explosion: Comparative study between different processes. *Carbohydrate Polymers, 290*, Article 119460. https://doi.org/10.1016/j.carbpol.2022.119460

Nepali, P., Suresh, S., Pikale, G., Jhaveri, S., Avanthika, C., Bansal, M., … Chanpura, A. (2022). Hypertension and the role of dietary fiber. *Current Problems in Cardiology, 47*(7), Article 101203. https://doi.org/10.1016/j.cpcardiol.2022.101203

Qiao, H., Shao, H., Zheng, X., Liu, J., Liu, J., Huang, J., … Guan, W. (2021). Modification of sweet potato (Ipomoea batatas Lam.) residues soluble dietary fiber following twin-screw extrusion. *Food Chemistry, 335*, Article 127522. https://doi.org/10.1016/j.foodchem.2020.127522

Shen, M., Ge, Y., Kang, Z., Quan, Z., Wang, J., Xiao, J., … Cao, L. (2019). Yield and physicochemical properties of soluble dietary fiber extracted from untreated and steam explosion-treated black soybean hull. *Journal of Chemistry, 2019*, 1–9. https://doi.org/10.1155/2019/9736479

Si, J., Yang, C., Ma, W., Chen, Y., Xie, J., Qin, X., … Yu, Q. (2022). Screen of high efficiency cellulose degrading strains and effects on tea residues dietary fiber modification: Structural properties and adsorption capacities. *International Journal of Biological Macromolecules, 220*, 337–347. https://doi.org/10.1016/j.ijbiomac.2022.08.092

Spann, R., & Boucher, D. (2022). Impact of molecular weight on the solubility parameters of poly (3-hexylthiophene). *Journal of Polymer Science, 1–12*. https://doi.org/10.1002/pol.20220573

Turner, N. D., & Lupton, J. R. (2021). Dietary fiber. *Advances in Nutrition, 12*(6), 2553–2555. https://doi.org/10.1093/advances/nmab116

Waddell, I. S., & Orfila, C. (2022). Dietary fiber in the prevention of obesity and obesity-related chronic diseases: From epidemiological evidence to potential molecular mechanisms. *Critical Reviews in Food Science and Nutrition, 1–16*. https://doi.org/10.1080/10408398.2022.2061909

Wan, F., Feng, C., Luo, K., Cui, W., Xia, Z., & Cheng, A. (2022). Effect of steam explosion on phenolics and antioxidant activity in plants: A review. *Trends in Food Science & Technology, 124*, 13–24. https://doi.org/10.1016/j.tifs.2022.04.003

Wang, J., Shi, S., Li, F., Du, X., Kong, B., Wang, H., & Xia, X. (2022). Physicochemical properties and antioxidant activity of polysaccharides obtained from sea cucumber gonads via ultrasound-assisted enzymatic techniques. *LWT, 160*. https://doi.org/10.1016/j.lwt.2022.113307

Wang, T., Liang, X., Ran, J., Sun, J., Jiao, Z., & Mo, H. (2017). Response surface methodology for optimisation of soluble dietary fibre extraction from sweet potato residue modified by steam explosion. *International Journal of Food Science & Technology, 52*(3), 741–747. https://doi.org/10.1111/ijfs.13329

Yang, C., Ma, Y., Chen, Y., Xie, J., Hu, X., & Yu, Q. (2022). Improving the physicochemical and in vitro hypolipidemic properties of soluble dietary fiber in camellia seed residue by a cellulose degrading fungus YC49. *Food & Function, 13*(21), 11321–11333.

Zhai, X., Ao, H., Liu, W., Zheng, J., Li, X., & Ren, D. (2022). Physicochemical and structural properties of dietary fiber from Rosa roxburghii pomace by steam explosion. *Journal of Food Science and Technology, 59*(6), 2381–2391. https://doi.org/10.1007/s13197-021-05254-7

Zhang, Y., Feng, Y., Shi, H., Ding, K., Zhou, X., Zhao, G., & Hadiatullah, H. (2022). Impact of steam explosion pretreatment of defatted soybean meal on the flavor of soy sauce. *LWT, 156*. https://doi.org/10.1016/j.lwt.2021.113034

Zhao, M., Guan, Z., Tang, N., & Cheng, Y. (2023). The differences between the water-and alkaline-soluble Poria cocos polysaccharide: A review. *International Journal of Biological Macromolecules*. , Article 123925. https://doi.org/10.1016/j.ijbiomac.2023.123925

Zhao, Y., Yu, K., Tian, X., Sui, W., Wu, T., Wang, S., … Zhang, M. (2022). Combined modification of soluble dietary fibers from Apple Pomace by steam explosion and enzymatic hydrolysis to improve its structural, physicochemical and functional properties. *Waste and Biomass Valorization, 13*(12), 4869–4879. https://doi.org/10.1007/s12649-022-01823-9

Zhang, G., Hao, M., He, Y., Ahmad, I., Ding, Y., & Lyu, F. (2023). Structural, physicochemical, and functional properties of insoluble dietary fiber derived from okara by Viscozyme® L. *Journal of Food Science, 88*, 1994–2008.

Zheng, Y., Wang, X., Tian, H., Li, Y., Shi, P., Guo, W., & Zhu, Q. (2021). Effect of four modification methods on adsorption capacities and in vitro hypoglycemic properties of millet bran dietary fibre. *Food Research International, 147*, Article 110565. https://doi.org/10.1016/j.foodres.2021.110565

Zheng, Y., Xu, B., Shi, P., Tian, H., Li, Y., Wang, X., … Liang, P. (2022). The influences of acetylation, hydroxypropylation, enzymatic hydrolysis and crosslinking on improved adsorption capacities and in vitro hypoglycemic properties of millet bran dietary fibre. *Food Chemistry, 368*, Article 130883. https://doi.org/10.1016/j.foodchem.2021.130883

Zhu, R., Xu, T., He, B., Wang, Y., Zhang, L., & Huang, L. (2022). Modification of artichoke dietary fiber by superfine grinding and high-pressure homogenization and its protection against cadmium poisoning in rats. *Foods, 11*(12), 1716. https://doi.org/10.3390/foods11121716